Mechanics of Advanced Composite Structures 4 (2017) 19-31

Semnan University

Mechanics of Advanced Composite Structures

journal homepage: http://MACS.journals.semnan.ac.ir

Study of Laminated Composite MEMS and NEMS Performance in Nano-metric Operations

S. Sadeghzadeh [a*], M.H. Korayem [b], A. Homayooni [b]

[a] *Smart Micro/Nano Electro Mechanical Systems Lab (SMNEMS), Nanotechnology Department, School of New Technologies, Iran University of Science and Technology, Tehran, Iran*

[b] *Robotic Research Laboratory, Center of Excellence in Experimental Solid Mechanics and Dynamics, School of Mechanical Engineering, Iran University of Science and Technology, Tehran, Iran*

PAPER INFO

Paper history:
Received 2016-08-12
Revised 2016-09-15
Accepted 2016-11-15

Keywords:
Laminated Composite
Micro electro mechanical systems
Nano electro mechanical systems
Generalized differential quadrature
Nano-manipulation

ABSTRACT

Precision of nano-metric operations is an important issue in nano-engineering studies. Several operative parameters might affect the quality of results. The parameters of the nano world are significant but not entirely controllable. However, the geometrical and mechanical properties of micro cantilevers are completely controllable. So, controlling the sensitivity of resulting image through t lamination design could be a proper approach. This paper analyses the effects of composite lamination on the performance of common Micro and Nano Electro Mechanical systems (MEMS and NEMS, respectively). Generalized Differential Quadrature (GDQ) and Generalized Differential Quadrature Element (GDQE) methods are used as semi-analytic solutions for regular and irregular domains, respectively. Validity, applicability and accuracy of the proposed approach are demonstrated and then the lamination effects on the nano-imaging and manipulation of nano particles by micro cantilevers are studied. This study shows that some laminations of micro cantilevers resulted in a better performance in nano-manipulation and imaging. Furthermore, clarifying the dependency of system sensitivity on the profile of the substrate is remarkable.

DOI: 10.22075/MACS.2016.495
© 2017 Published by Semnan University Press. All rights reserved.

1. Introduction

Sensing and actuating the small scales has trended the researchers to focus on Micro and Nano Electro Mechanical systems (MEMS and NEMS). However, experiment-based predictions are very expensive in this area. As a proper alternative, therefore, micro- and nano electro mechanics theories must be further developed and applied. Piezoelectric-based structures, named smart structures, are the most well-known category of MEMs and NEMs. Applications of piezoelectric actuators extend to the following things: mass production of sound transmitters; ultrasonic power transducers and sensors; bending actuators for textile machines; ink print heads; beam benders in valves, in braille displays, in optical systems; and newly monolithic multilayer actuators for automotive injection systems [1].

A sufficiently accurate model for MEMs and NEMs remains one of the most challenging problems of the MEMs and NEMs dynamics. Until now, numerical methods have been developed to study the dynamics of small devices, such as the finite element method (FEM), the finite difference method (FDM) and the finite cloud meshless method (FCM) [2-4]. This paper will show that although FEM is sufficiently simple and accessible, its precision is limited in some usual boundary and ambient conditions. As an alternative, Generalized Differential Quadrature (GDQ) and Generalized Differential Quadrature Element (GDQE) methods have been recently applied to continuous and discontinuous mechanical sys-

* Corresponding author. Tel.: +98-21-73225812; Fax: +98-21-73021482

E-mail address: sadeghzadeh@iust.ac.ir

tems, respectively. In this paper, these methods are used to study the performance of NEMs and MEMs in nanometric operations. It is useful to list valuable works on modelling nano-manipulation and nano-imaging with the molecular dynamics approach. Coarse-grained molecular dynamics simulation of the automatic nano-manipulation process was performed to study the effect of tip damage on the positioning errors [5]. However, nano-cluster manipulation's success in considering the flexibility of the system was studied via molecular dynamics simulations [6].

Some researchers have focused on the free vibration analysis of plates and shells as a common mechanical problem [7-9]. Others have presented the mechanics of especial systems through especial conditions [10]. Piezoelectric-based structures typically have complicated behavior due to multi-field excitations. This forces the implementation of numerical methods. Balamurugan and Narayanan [11] have used a nine-nodded, piezo-laminated, degenerated shell element to model and analyse multi-layered composite shell structures together with sensors and piezoelectric actuators. Applications of FEM in structures, including sensors and actuators, are surveyed [12]. In addition to FEM, advanced numerical methods have been developed. For instance, the differential quadrature method (DQM) has been introduced as an effective semi-analytic method in the analysis of the free, static and dynamic response of mechanical systems. Then some researchers have used it for more complicated mechanical engineering problems [13]. Other related works can be mentioned where the piezoelectric laminated cylindrical shell - with the shear rotations effect under the electromechanical loads and the four sides simply supported the boundary condition - was studied by using the two-dimensional generalized DQ (GDQ) computational method [14]. The application of DQ is limited to uniform domains, and for irregular domains, including the discontinuity in material or geometry, the DQ element method (DQEM) has been suggested by Chen [15]. Researchers believe that the GDQ and GDQE methods lead to moderately exact solutions to problems [16,17]. So, it could be a proper analysis procedure.

The imaging and manipulation of nano objects include various techniques performed by especial devices named macro-scale nano-robots [18]. Imaging and manipulation could be performed in various procedures based on the aims and goals of the operation [18]. Accuracy is the most significant challenge in such devices. Usually, nonlinearity has been observed in the MEMs and NEMs that are used in nano-robots. Predicting these nonlinearities is very useful to achieve sufficient accuracy for the operation. In this paper, nonlinearities were neglected and a linear model was proposed.

This paper represents a comprehensive semi-analytic approach for static and dynamic responses of nano-robots that could include torsion, elongation and bending in various planes. The most prominent contribution of this study is to comprehensively investigate the laminated composite effects on nano-manipulation and nano-imaging.

2. Problem

Piezoelectric materials could be used in various configurations for actuation and/or sensing purposes. For instance, the mono-morph, bimorph and tri-morph laminations are the most well-known representatives of piezoelectric plate-bending actuators. Multilayer technology has the advantage of working with even lower driving voltages. In this study, which uses laminated composite structures, a general and applicable configuration is suggested for a superior performance in MEMs and NEMs. The imaging and manipulation of nano objects by Scanning Probe Microscopes (SPMs) and especially an Atomic Force Microscope (AFM) are two of the prominent applications of micro-cantilevers. For example, the imaging of a surface and the manipulation of a nanoparticle are depicted in Figure 1 schematically.

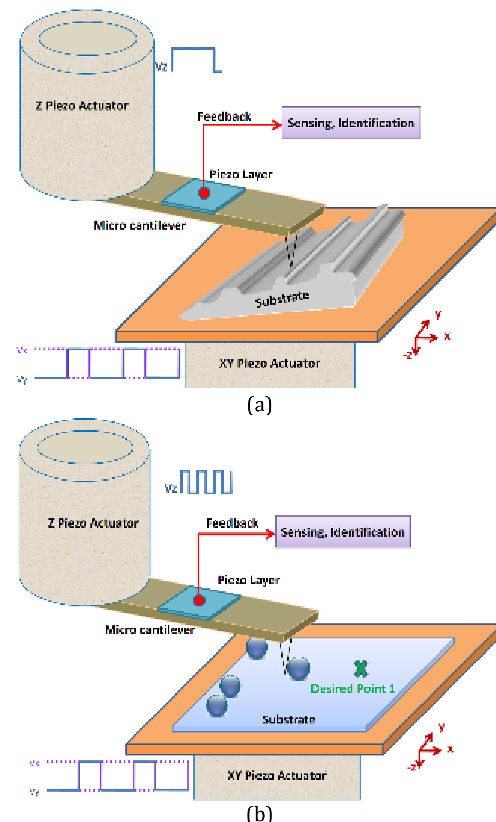

Figure 1. (a) Imaging of a general substrate and (b) manipulation of a nanoparticle by a general AFM.

As depicted in Figure 1, in an AFM, the micro-cantilever is attached at the end of a piezotube actuator. Since the dimensions of the micro-cantilever with respect to the piezo tube are negligible, the dynamics of the piezo tubes are neglected. Recently, the dynamics of a piezo tube in nano-imaging and manipulation operations have been studied [16].

2.1. Formulation of micro-cantilever dynamics

The general form of the linear constitutive relation of piezo-electro mechanics can be written as:

$$D=[e]\{S\}-[\in]\{E\}$$
$$\sigma=[C]\{S\}-[e]^{T}\{E\} \tag{1}$$

where [C], [e] and $[\in]$ denote the elastic coefficients, piezoelectric constant and dielectric permittivity matrices, respectively [16,17].

Based on the dimensions of the MEMs and NEMs used, mentioned previously, the laminated system considered is assumed to be thin and, thus, strains along the thickness can be neglected. Here, the First Order Shear Deformation Theory (FSDT) is used. Using the generalized Hamilton principle, the equations of motion and related boundary conditions of a segmented laminated shell are derived as:

$$\left.\frac{\partial N_{xx}}{\partial x}+\frac{\partial N_{xy}}{\partial y}+F_x^*=I_1\ddot{u}+I_2\ddot{\phi}_1\right]^i$$
$$\left.\frac{\partial N_{xy}}{\partial x}+\frac{\partial N_{yy}}{\partial y}+F_y^*=I_1\ddot{v}+I_2\ddot{\phi}_2\right]^i$$
$$\left.\frac{\partial Q_{xz}}{\partial x}+\frac{\partial Q_{yz}}{\partial y}+N(w_0)+F_z^*=I_1\ddot{w}\right]^i \tag{2}$$
$$\left.\frac{\partial M_{xx}}{\partial x}+\frac{\partial M_{xy}}{\partial y}-Q_{xz}+Q_{xz}^*=I_2\ddot{u}+I_3\ddot{\phi}_1\right]^i$$
$$\left.\frac{\partial M_{xy}}{\partial x}+\frac{\partial M_{yy}}{\partial y}-Q_{yz}+Q_{yz}^*=I_2\ddot{v}+I_3\ddot{\phi}_2\right]^i$$

in which I_i is the inertia and $N(w_0)$ is the nonlinear term of equations whose higher-order terms are neglected.

$$N(w_0)=\frac{\partial}{\partial x}(N_{xx}\frac{\partial w_0}{\partial x}+N_{xy}\frac{\partial w_0}{\partial y})+\frac{\partial}{\partial y}(N_{yy}\frac{\partial w_0}{\partial y}+N_{xy}\frac{\partial w_0}{\partial x}) \tag{3}$$

It is particularly important for an actuator that the stiffness of the system is affected by the nonlinear term. In the equations presented, the upper asterisks (*) denote the external forces. In MEMs and NEMs, there is an electric field beneath the bigger surfaces and, thus, there is current along the thickness (E_z). Using the electroelastic charge equation and the boundary condition, the electric potential can be written as:

$$E_{zk}]^i=\left[-\frac{Q_{3k}}{\in_{33k}}-\frac{(\bar{e}_{31k}\bar{S}_{xx}+\bar{e}_{32k}\bar{S}_{yy}+\bar{e}_{36k}\bar{S}_{xy})}{\in_{33k}}\right]^i \tag{4}$$

where Q_{3k} is the surface electric charge density of the kth layer in i^{th} segment. The piezoelectric force and moment resultants N^e and M^e are defined as:

$$\left.\begin{Bmatrix}\{N^e\}_{3\times1}\\ \{M^e\}_{3\times1}\end{Bmatrix}\right]^i=\left.\sum_{k=1}^{M}\int_{\zeta_{k-1}}^{\zeta_k}[e]\begin{Bmatrix}\{\sigma_k^{elec}\}^T\\ \zeta\{\sigma_k^{elec}\}^T\end{Bmatrix}d\zeta\right]^i \tag{5}$$

where $\{\sigma_k^{elec}\}^i=\{\bar{e}_{31}\ \bar{e}_{32}\ \bar{e}_{36}\}_k^i E_{zk}^i$ and "M" is the number of piezoelectric layers. Based on the theory mentioned, for each element, the equation of motion, in operator form, can be written as:

$$\left[L_j^{mech}(u,v,w,\phi_1,\phi_2)\right]^i+\left[L_j^{elec}(u,v,w,\phi_1,\phi_2,\Phi)\right]^i+q_j^i=I_j^i\ddot{u}_j^i \tag{6}$$

where $L_i^{mech}(u,v,w,\phi_1,\phi_2)$ and $L_i^{elec}(u,v,w,\phi_1,\phi_2,\Phi)$ are the mechanical and electrical effects, respectively, and I_j^i is the mass term of the jth equation for i^{th} element. The electrical effect contains two parts: the converse effect $(L_i^{Celec}(\Phi))$, and the direct effect $(L_i^{Delec}(u,v,w,\phi_1,\phi_2,\Phi))$. The geometrical compatibility conditions at the common nodes of the two connected elements are defined as:

$$\left(u^{(i+1)}-u^{(i)}\right)=0,\ \left(v^{(i+1)}-v^{(i)}\right)=0,$$
$$\left(w^{(i+1)}-w^{(i)}\right)=0,\left(\phi_1^{(i+1)}-\phi_1^{(i)}\right)=0, \tag{7-a}$$
$$\left(\phi_2^{(i+1)}-\phi_2^{(i)}\right)=0$$

Denoting the axial and circumferential directions by "x" and "y," respectively, the natural compatibility conditions are as follows:

$$\left(N_y^{(i+1)}-N_y^{(i)}\right)\Big|_{y=Ly^{(i)}}=0$$
$$\left(N_{xy}^{(i+1)}-N_{xy}^{(i)}\right)\Big|_{y=Ly^{(i)}}=0$$
$$\left(M_y^{(i+1)}-M_y^{(i)}\right)\Big|_{y=Ly^{(i)}}=0 \tag{7-b}$$
$$\left(M_{xy}^{(i+1)}-M_{xy}^{(i)}\right)\Big|_{y=Ly^{(i)}}=0$$
$$\left(Q_y^{(i+1)}-Q_y^{(i)}\right)\Big|_{y=Ly^{(i)}}=0$$

$$\left(N_x^{(i+1)}-N_x^{(i)}\right)\big|_{x=Lx^{(i)}}=0$$
$$\left(N_{xy}^{(i+1)}-N_{xy}^{(i)}\right)\big|_{x=Lx^{(i)}}=0$$
$$\left(M_x^{(i+1)}-M_x^{(i)}\right)\big|_{x=Lx^{(i)}}=0 \quad (7\text{-c})$$
$$\left(M_{xy}^{(i+1)}-M_{xy}^{(i)}\right)\big|_{x=Lx^{(i)}}=0$$
$$\left(Q_x^{(i+1)}-Q_x^{(K)}\right)\big|_{x=Lx^{(i)}}=0$$

Also, the natural and geometrical external boundary conditions along the x and y edges are:

$$u=u_0 \quad Or \quad N_x=N_{x0}$$
$$v=v_0 \quad Or \quad N_{xy}=N_{xy0}$$
$$w=w_o \quad Or \quad Q_x=Q_{x0}$$
$$\varphi_1=\varphi_1^0 \quad Or \quad M_x=M_{x0}$$
$$\varphi_2=\varphi_2^0 \quad Or \quad M_{xy}=M_{xy0}$$
$$v=v_0 \; Or \; N_y=N_{y0}$$
$$u=u_0 \; Or \; N_{xy}=N_{xy0}$$
$$w=w_o \; Or \; Q_y=Q_{y0} \quad (7\text{-d})$$
$$\varphi_2=\varphi_2^0 \; Or \; M_y=M_{y0}$$
$$\varphi_1=\varphi_1^0 \; Or \; M_{xy}=M_{xy0}$$

3. Solution

In numerical analyses, a specific feature makes GDQ and GDQE highly distinctive in reaching very precise results by using merely a few grid points. This feature, which will be introduced in the following notes, is particularly precious in structural and vibration applications. In principle, DQM was initially introduced to express the derivatives of a function to various directions in terms of the sum of weighted function values at some specific discrete points.

$$\left.\frac{\partial^n f(x_1,\ldots,x_i,\ldots,x_p)}{\partial x_i^n}\right|_{x_i=X_i}= \quad (8)$$
$$\sum_{j=1}^{N} w_{ij}^n \, f(x_1,\ldots,X_i,\ldots,x_p) \quad (i=1:N)$$

In Eq. (8), x_i, n, N, f, X_i and W_{ij}^n denote coordinate system directions (such as a curvilinear one), order of derivative, number of discrete points, desired function, points in the x_i direction whose derivatives are needed, and weighting coefficients (for nth order derivative in the x_i direction and at point X_i), respectively. Recently, a recursive relation has been developed to calculate the weighting coefficients as [14]:

$$\begin{Bmatrix} w_{ij}^{(m)}=m\left[a_{ij}w_{ij}^{(m-1)}-\dfrac{w_{ij}^{(m-1)}}{x_i-x_j}\right] \\ (i\neq j) \quad (i,j=1:N;\; m=2:N-1) \end{Bmatrix} \quad (9\text{-a})$$
$$\begin{Bmatrix} w_{ii}^{(m)}=-\sum_{j=1,\,j\neq i}^{N} w_{ij}^{(m)} \\ (i=j) \quad (i,j=1:N) \end{Bmatrix}$$

where a_{ij} are the first derivative coefficients, calculated by [14] as:

$$\begin{cases} a_{ij}=\dfrac{M^{(1)}(x_i)}{(x_i-x_j).M^{(1)}(x_j)} & (i\neq j) \\ a_{ii}=-\sum\limits_{j=1,\,j\neq i}^{N} a_{ij} & (i=j) \end{cases} \quad (9\text{-b})$$

Note that $M^{(1)}(x_i)=\prod_{k=1,k\neq i}^{N}(x_i-x_k)$. For numerical calculations, sampling points with the Chebyshev-Gauss-Lobatto are employed in the following way:

$$x_i=\frac{L}{2}\left(1-Cos\frac{(i-1)\pi}{N-1}\right) \;,\; i=1,2,\ldots,N \quad (10)$$

where L is the specific length along the direction considered. Due to the discontinuity, domain decomposition is needed for segmented systems. Therefore, various elements should be considered and the GDQEM should be applied. Generally, neglecting the damping effect, equations of motion yield:

$$\begin{aligned} &L_i^{mech}(U,V,W,\Phi_1,\Phi_2) \\ &+L_i^{Delec}(U,V,W,\Phi_1,\Phi_2) \\ &+F_{extI}=\mathrm{I}_j^i\{\ddot{U},\ddot{V},\ddot{W},\ddot{\Phi}_1,\ddot{\Phi}_2\}^T \end{aligned} \quad (11)$$

And the boundary conditions are defined as:

$$\begin{aligned} &B_k^{mech}(U,V,W,\Phi_1,\Phi_2) \\ &+B_k^{Delec}(U,V,W,\Phi_1,\Phi_2)=F_{extB} \end{aligned} \quad (12)$$

where, F_{extI} and F_{extB} are the vectors of external forces on interior and boundary points, respectively.

For the implementation of boundary conditions in the DQM or DQEM, several approaches have been proposed. Except for the general approach [14], others cannot be used in cases other than those that are simply supported or have clamped conditions. The equations of motion and boundary conditions can be rewritten in the matrix form as:

$$\begin{aligned} &A_{IB}W_B+A_{II}W_I=\Omega_I\ddot{W}_I+F_{Dist} \\ &A_{BB}W_B+A_{BI}W_I=F_{BC} \end{aligned} \quad (13)$$

where F_{Dist} and F_{BC} are the distributed forces of the interior and boundary forces that are obtained

from F_{extI} and F_{extB}. Substituting W_B from the second into the first relation in Eq. 13 leads to:

$$\ddot{W}_I = \Omega_I^{-1}(A_{II} - A_{IB}A_{BB}^{-1}A_{BI})W_I - \Omega_I^{-1}F_{Dist} + \Omega_I^{-1}A_{IB}A_{BB}^{-1}(F_{BC}) \quad (14)$$

And in the state space form:

$$\begin{Bmatrix} \dot{W}_I \\ \ddot{W}_I \end{Bmatrix} = \begin{bmatrix} 0 & I \\ \Omega_I^{-1}(A_{II} - A_{IB}A_{BB}^{-1}A_{BI}) & 0 \end{bmatrix} \begin{Bmatrix} W_I \\ \dot{W}_I \end{Bmatrix} + \begin{Bmatrix} 0 \\ -\Omega_I^{-1}(F_{Dist} + A_{IB}A_{BB}^{-1}F_{BC}) \end{Bmatrix} \quad (15)$$

Using a numerical approach, for instance, the Runge-Kutta method, the aforementioned state space equation can be solved. Then displacement of boundary points can be calculated as

$$W_B = A_{BB}^{-1}(F_{BC} - A_{BI}W_I) \quad (16)$$

For static problems, the solution of Eq. (13) can be written as:

$$W_I = (A_{II} - A_{IB}A_{BB}^{-1}A_{BI})^{-1}(F_{Dist} - A_{IB}A_{BB}^{-1}F_{BC}), \quad W_B = A_{BB}^{-1}(F_{BC} - A_{BI}W_I) \quad (17)$$

4. Validation

4.1. Comparison of static deflections

Numerical solutions exist for electromechanical problems. The Finite Element Method (FEM) is commonly used to study the behavior of MEMs and even NEMs. Previously, validation used to be provided by the comparison of methods with the traditional software programs, such as ANSYS and ABAQUS. Here, for more clarification, comparisons of the static and dynamic responses are made with the Green's function approach and ANSYS software. In ANSYS, the shell element has been used. These types of comparisons clearly show the efficiency of the proposed model. Table 1 lists the properties and dimensions of beams and plates used for the comparison. Table 2 lists the static deflection of the midpoint of the beam and plate due to the point and uniformly distributed loads. For each problem, the simulation error of GDQM is of a considerably lower order compared to that of FEM. Table 2 also lists the comparison of the static deflection of a stepped B-beam, due to the 100 N point and uniform loads using GDQEM. Furthermore, due to a 100 N uniform line load on the step position, the static deflection of the midpoint of a B-plate is compared.

4.2. Comparison of dynamic response

The dynamic response of an A-beam (middle point) under the SS-SS boundary conditions due to a uniformly distributed load (as 100×Sin(10×t)) is depicted and compared for three different approaches in Figure 2. Figure 3 shows the dynamic response of an A-plate (middle point) under SS-SS-SS-SS boundary conditions, due to a uniformly distributed load (as 100×Sin(10×t)). In Figure 2, three approaches resulted in the same responses, when in the case of plate (Figure 3), the GDQ method leads to a more precise estimation.

Table 1. Properties of beams and plates used for simulations.

Problem	Dimensions (m)	Module of Elasticity (GPa)	Density (Kg/m^3)	Configuration
A-Beam	5×0.04×0.04	70	2,800	Simple
B-Beam	2.5×0.04×0.04,2.5×0.04×0.06	70	2,800	Step
A-Plate	1×1×0.03	70	2,800	Simple
B-Plate	0.5×1×0.03,0.5×1×0.05	70	2,800	Step
Problem	Dimensions (m)	Piezo Type	Material	Configuration
C-Plate	0.1×.05×.0025	PZT-5H	Gr/Epoxy	Simple
D-Plate	0.05×0.05×0.0025, 0.05×0.05×0.0015	PZT-5H	Gr/Epoxy	Step

Table 2. Comparison between the results of present approach, exact solution and ANSYS for static problem.

System and BC	Loading	Exact	ANSYS		GDQM	
			δ	Er. (Ans-Exct) (%)	δ	Er. (DQ-Exct) (%)
A-Beam, SS-SS	Point load on mid	17.43861607	17.386 mm	0.301720	17.43861 mm	0.000
A-Beam, SS-SS	Distributed Load	54.49567000	54.278 mm	0.399430	54.49567 mm	0.000
A-Plate, SS-SS-SS-SS	Distributed Load	2.34713e-3	2.5654e-3 mm	9.299442	2.35808e-3 mm	0.466

System and BC	Loading	ANSYS	GDQEM	Er. (Ans-DQ) (%)
B-Beam, C-F	Point load on end	0.0258350 m	0.025834986 m	0.0
B-Beam, C-SS	Point load on mid	0.0040965 m	0.004108690 m	0.3
B-Beam, C-C	Point load on mid	0.0025456 m	0.002558450 m	0.5
B-Beam, C-F	uniform line load	0.1785600 m	0.178019000 m	0.3
B-Beam, C-SS	uniform line load	0.0120030 m	0.012003150 m	0.0
B-Beam, C-C	uniform line load	0.0063912 m	0.006396139 m	0.0
B-Plate, C-C-C-F	uniform line load	1.0852000 µm	1.113778000 µm	2.0
B-Plate, C-C-C-C	uniform line load	0.6929000 µm	0.711344000 µm	2.0
B-Plate, C-SS-SS-C	uniform line load	1.0432000 µm	1.07712000 µm	3.1

As a result, according to the more accurate GDQ, it is used for the dynamic response in nanometric operations. As already discussed, the exact solution cannot be provided in the case of other boundary conditions. But the GDQ results could be compared with FEM with an intrinsic guarantee in accuracy for both static and dynamic responses.

Figure 4 shows the dynamic response of the stepped B-plate (middle point) under various boundary conditions and due to the uniformly distributed load (100×Sin(10×t)) applied to the patch. Obviously, in this figure, the GDQE results are close to those of ANSYS. However, it has already been demonstrated that the response of GDQE is more accurate.

Based on the aforementioned comparison, the reliability of the approaches presented is satisfied. Thus, it can be used to study the effects of various parameters on the performance of MEMs and NEMs. Here, for instance, the micro-cantilever (MC), which is used in nano-robots, is studied. The statics and dynamics of MC in the nano-imaging and manipulation of nano-particles have been discussed.

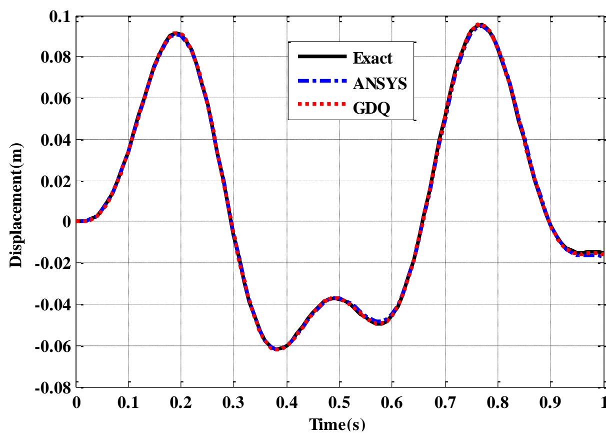

Figure 2. Dynamic response for a beam; comparison of exact, ANSYS and GDQ models.

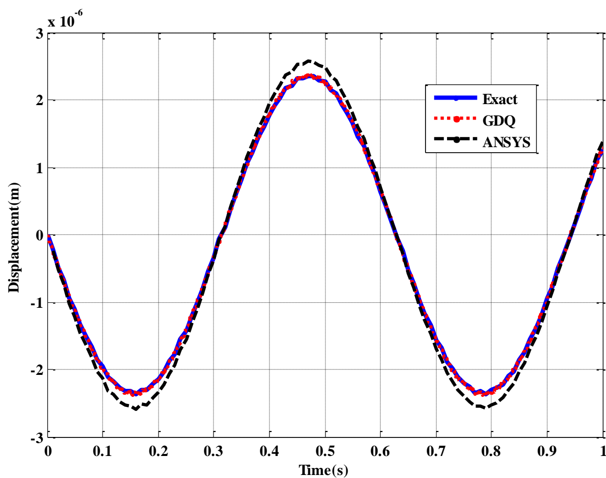

Figure 3. Dynamic response for a plate; comparison of exact, ANSYS and GDQM.

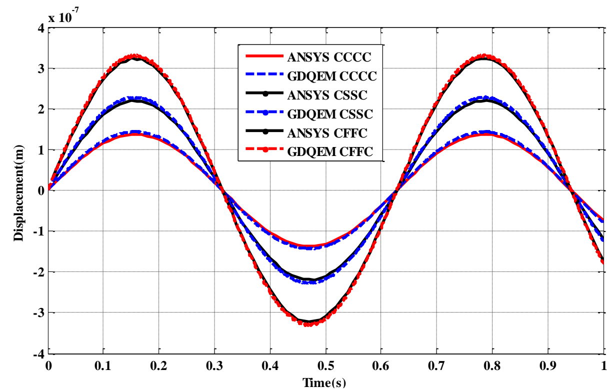

Figure 4. Dynamic response of the stepped B-plate (middle point) under various boundary conditions and due to the uniform 100sin(10t) distributed load applied on the patch.

4. Results and Discussion

There are two key operations in nano-scale in which the micro-cantilever plays an important role: nano-imaging and nano-manipulation. These two operations are discussed in the next sections as the most useful results could be concluded.

5.1. Surface nano-imaging

Precision of nanoimaging is an important issue in nano-engineering studies. Various parameters affect the quality of images obtained. Parameters in the nano-world, such as roughness of surface and chemical properties, are the most significant, but they are not entirely controllable. However, are some parameters in macro world could be changed and controlled. For instance, the geometrical and mechanical properties of micro-cantilevers could seriously affect the imaging result. So controlling the sensitivity of resulting image through the lamination design could be a proper approach. Figure 5 shows the nano-imaging scheme. Recently, by implementing molecular dynamics, a shape feedback has been used to control the shape of a particle used in manipulating [19]. Here, the problem is considered to be a state-dependent dynamic force on the MC end. Neglecting the tip deformation effects on the dynamics of MC, where they might be studied via molecular dynamics, Figure 6 shows the algorithm implemented. An interaction-attraction force field is considered for the interfacial force between the tip end and substrate [20]:

where “a” and “b” are the force coefficients and “u” is the deflection of the MC end. The quantities of “a” and “b” depend on the system considered. The best evaluation of “a” can be provided through the inverse of the amplitude of the MC end (a□1/□). And “b” can be considered 1 (one). For simplicity, a general profile is assumed for the substrate, including triangular, square and sinusoidal parts, simultaneously. The desired and resulting profiles, obtained

by the first configuration depicted in Figure 7, are illustrated on the left side of Figure 5. The length, width and thickness are 200, 40 and 8 micrometers, respectively.

$$F = -\frac{a}{u} + \frac{b}{u^2} \tag{18}$$

$$\frac{d}{dt}\begin{Bmatrix} W_I \\ \dot{W}_I \end{Bmatrix} = \begin{bmatrix} 0 & I \\ \Omega_I^{-1}(A_{II} - A_{IB}A_{BB}^{-1}A_{BI}) & \Omega_I^{-1}(C_{IB}A_{BB}^{-1}A_{BI} - C_{II}) \end{bmatrix} \begin{Bmatrix} W_I \\ \dot{W}_I \end{Bmatrix} + \begin{Bmatrix} 0 \\ \Omega_I^{-1}C_{IB}A_{BB}^{-1}\dot{F}_{BC} - \Omega_I^{-1}F_{Dist} + \Omega_I^{-1}A_{IB}A_{BB}^{-1}(F_{BC}) \end{Bmatrix} \tag{19}$$

To evaluate the lamination composite effects on the imaging results, the third configuration of lamination, demonstrated in the left side of Figure 5, is studied with various laminations. Assuming a proportional damping, Figure 8 shows the effects of various laminations on the nano-imaging result by scanning the above-mentioned general profile. Implementing proportional damping into Eq. (15) leads to Eq. (19), where, C_{IB} and C_{II} have been selected as:

$$\begin{aligned} C_{IB} &= PDC(\eta A_{IB} + \gamma \rho_{average} U_{IB}) \\ C_{II} &= PDC(\eta A_{II} + \gamma \rho_{average} U_{II}) \end{aligned} \tag{20}$$

PDC, $\rho_{average}$ and U are the total proportional damping coefficient, average density of lamination and identity matrix, respectively. The constant coefficients η and γ are assumed to be 0.0008 and 0.0003. For more clarification, some subplots of Figure 8 have been enlarged in Figure 9. The legend of Figure 9 is mentioned in Figure (9-e). The key areas focused on in Figure 9 could be used to study the output sensitivity of various configurations to obtain more precise results. When same geometrical, ambient and imaging schemes are used, one expects to observe different results for the profile obtained because of the variations in stiffness in the laminations used. Thus, some behavior is mechanically predictable and simulations are not necessary. In practice, however, some factors limit the performance of MEMS and NEMS. Thus, even smallest difference between various laminations may lead to an optimal selection of lamination for more precise imaging. The P/90˚/0˚/P lamination results in more precision in the case of the ascent (Figure 9-a), peak (Figure 9-b) and descent (Figure 9-c) parts of the triangular surface. Fr square and sinusoidal profiles, the output image is completely different. The P/90˚/0˚/P lamination leads to the worst results. Based on the fourth to sixth subplots of Figure 9, the P/0˚/0˚/0˚/P lamination is suggested for square and sinusoidal profiles. The dependency of system sensitivity on the profile of a substrate is a highly significant result in imaging especial surfaces. Among all laminations studied, P/90˚/0˚/P and P/0˚/0˚/0˚/P are suggested for triangular and both square and sinusoidal substrates, respectively.

Figure 8 is provided by using a sufficient damping coefficient. Piezoelectric shunt damping is a well-known technique for suppressing vibration in MEMS and NEMS. Techniques encompassed in this broad description are characterized by connecting electrical impedance to a structurally bonded piezoelectric transducer [21]. Such methods can guarantee the stability of the shunted system without any external sensor and do not require parametric models for a design. Thus, by using an electrical circuit, proportional damping could be designed to achieve the desired behavior. With this assumption, using the P/30/0/-30/P lamination for scanning a simpler substrate profile (as demonstrated in Figure 10), the effects of PDC on the image obtained are depicted in Figure 10. As illustrated in this figure, for a better result, the damping should be in an especial range. For instance, the PDC between 0.0001 and 0.001 could be acceptable. The real like three-dimensional (3D) image of scanned surface could be obtained by repeatedly scanning the substrate considered. The real and 3D images of substrate obtained for three PDCs are shown in Figure 11.

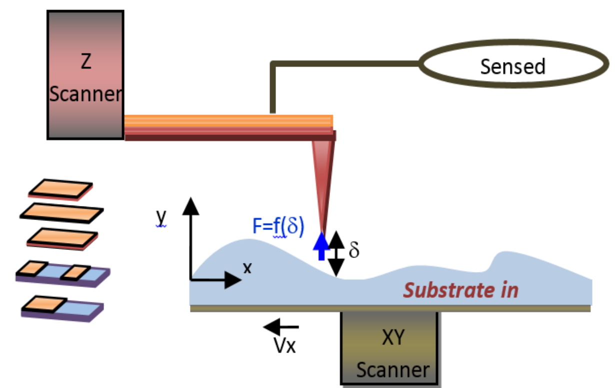

Figure 5. Various configurations of MC and AFM nano-imaging scheme using the MC.

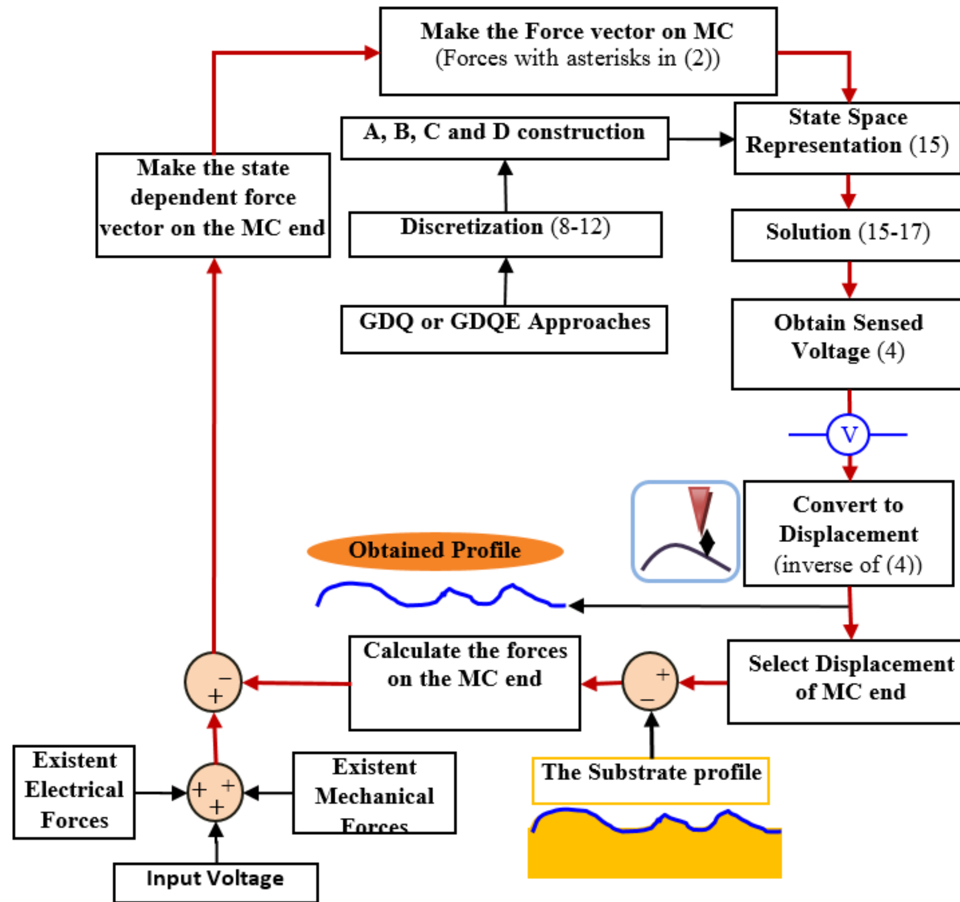

Figure 6. Imaging of a substrate using the GDQ and GDQE methods.

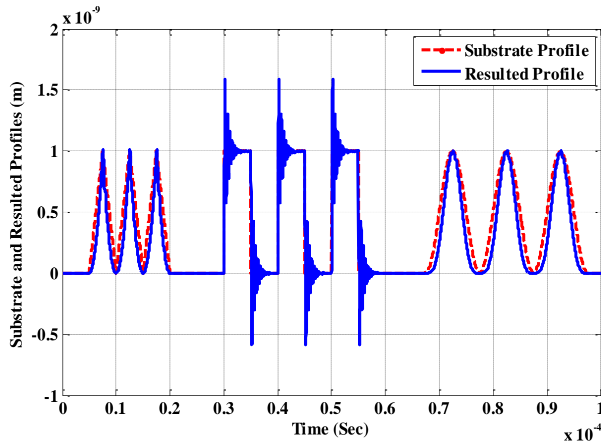

Figure 7. Substrate (real) and resulted profiles with a bimorph MC.

The substrate considered is similar to the one in Figure 11-a. The profile that resulted from using the algorithm presented with PDC = 0.0001 is demonstrated in the second picture of Figure 11 (11-b). Even though the triangular and sinusoidal parts are almost close to the profile of substrate, the ascent and descent parts of square profile are completely different. A less damping coefficient leads to deviations in the ascent and descent parts. However, as illustrated in the third picture, a more damping coefficient leads to unwanted delays. As the best result, the fourth picture (PDC = 0.0005) could be mentioned. Triangular, square and sinusoidal parts have been scanned and sketched precisely. These important issues could be used to improve the shunt damping technique to provide a more precise image of the substrate.

5.2. Manipulation of nano-particles

Scanning Probe Microscopes (SPMs) and especially the Atomic Force Microscope (AFM) are used to reach, identify and manipulate nano-objects. Depending on its configuration, an AFM could include one or two piezo-tube actuators that are about 10 mm to 15 mm long. The effects of the particle size on the semistatic deflection and sensed voltage of MC are studied here. Figure 12 shows a very special case of AFM, where one piezo-tube is used to span three dimensions in space. At the end of the piezo-tube, an MC is attached (with the length, width and thickness of about 200 μm, 8 μm and 1 μm, respectively), including a small conical tip (with the end diameter of about 10 nm) at the end. The piezo-tube scans the substrate in all directions (x, y and z).

Assuming the rigidity of the piezo-tube toward the MC, the dominant dynamics belong to the MC. CFFF boundary conditions could be considered for

the MC and the existing forces and moments on the end of the MC (Figure 13) are depicted in Figure 14 versus various steps of manipulation.

The effective forces in the nano-manipulation operation can be obtained by using certain formulations [16]. Figure 15 shows these results. The calculations are carried out in two cases, a particle with 20 nm (D20) and 100 nm (D100) of diameter. Forces in Cartesian coordinates and the free body diagrams for MC in the nano-manipulation mode are depicted in Figure 13. Table 3 lists forces and moments quantitatively for all steps of nano-manipulation.

Figure 15 shows the maximum of deflection of the MC in the various steps of nano-manipulations. The sensed voltage on the sensor layer of the MC is displayed in Figure 16. The effect of particle size on the static deflection and sensed voltage can be observed clearly. The bigger the particle used is, the bigger the resulting deflection and voltage are. The effects of lamination on the deflection and sensed voltage of MC can be observed clearly. The total thickness for all configurations considered is the same. The diagrams presented show that when two mechanical layers are used, the static deflection is greater. The P/0°/90°/P lamination leads to the greatest deflection and the minimum deflection belongs to the P/0°/0°/0°/P lamination. One should note that the deflections for D20 and D100 problems are approximately the same before step "E." Before this, the moments were zero and, thus, various laminations lead to approximately the same results in two cases.

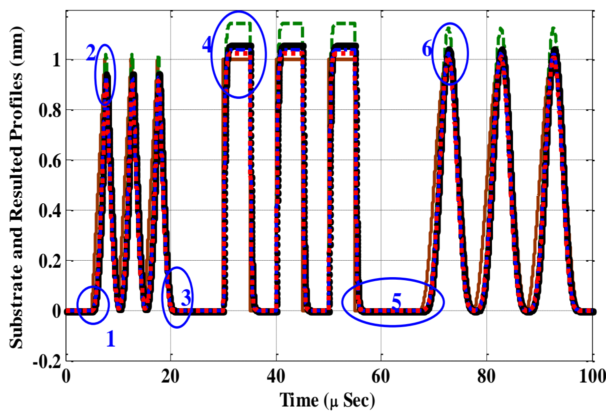

Figure 8. The resulting profile of various configurations for MC.

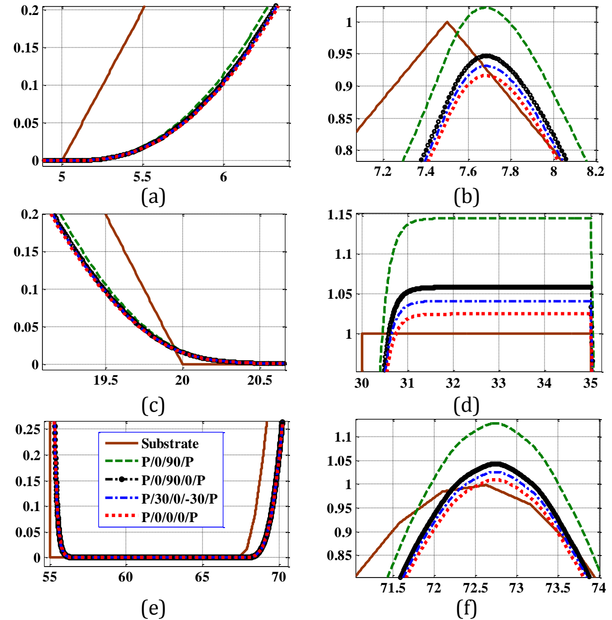

Figure 9. Some subplots of the resulted profile in various configurations.

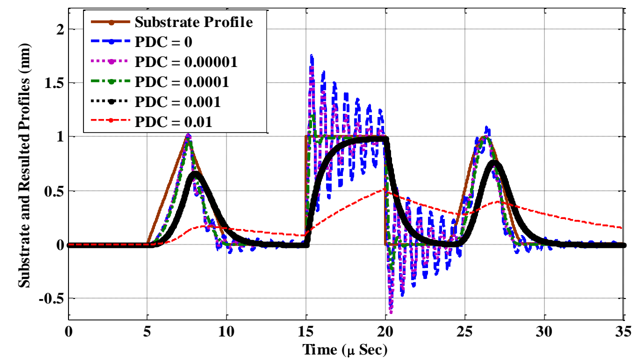

Figure 10. The damping effects on the resulting profile.

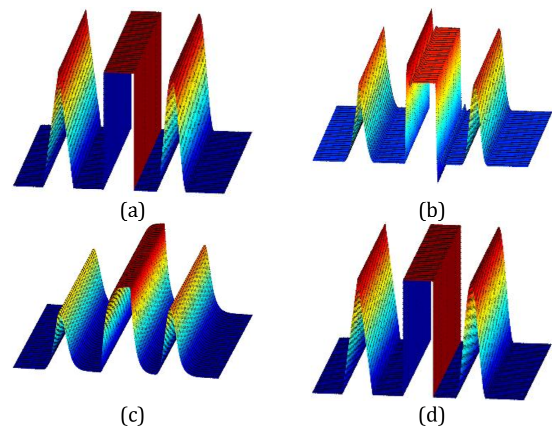

Figure 11. 3D view of (a) profile of substrate, (b) resulting profile by PDC=0.0001, (c) resulting profile by PDC=0.001 and (d) the best resulting profile by PDC=0.005.

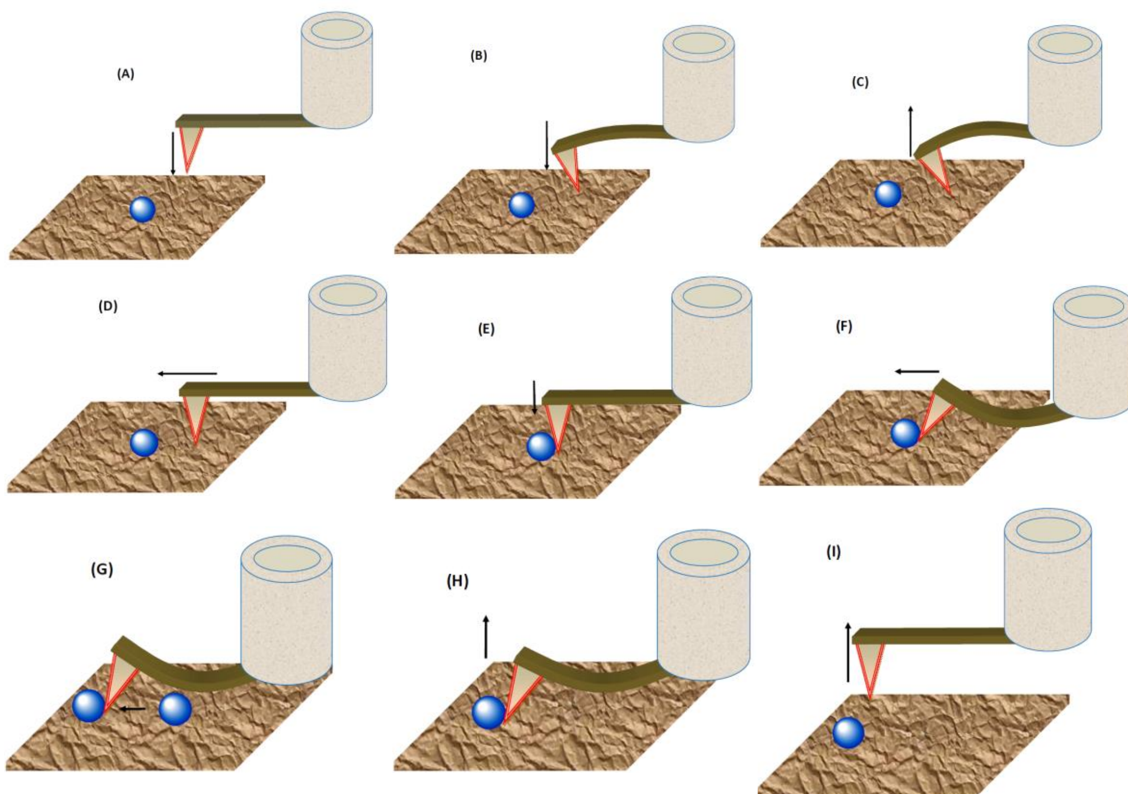

Figure 12. Manipulation strategy using the AFM: a) auto parking, b) snap in substrate, c) substrate pull out, d) approach to nanoobject, e) snap in nanoobject, f) offset in the z direction, g) pushing, h) nanoobject pull out, i) retraction [16].

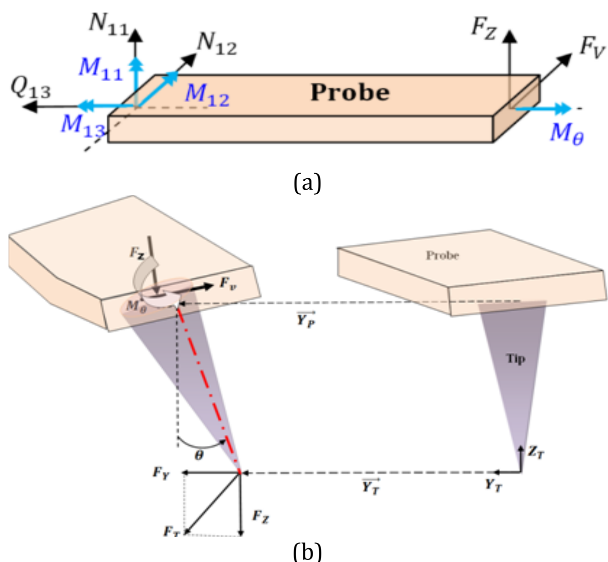

Figure 13. (a) The free body diagram for MC in nano-manipulation mode and (b) the tip and corresponding parameters [16].

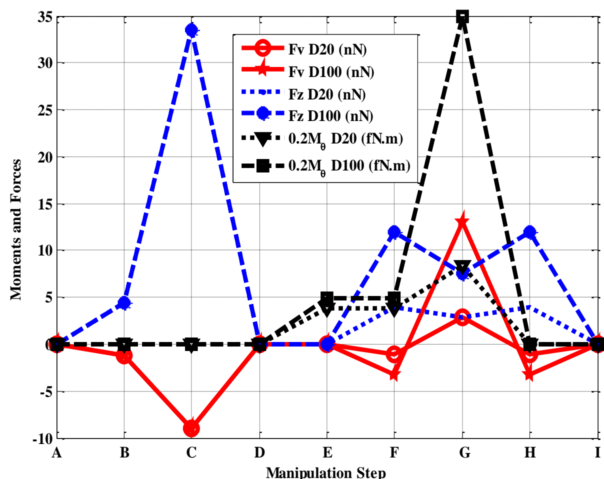

Figure 14. Significant forces and moments at the end of MC in the nano-manipulation strategy [16].

Table 3. The deflections of MC during the nano-manipulation of a nanoparticle

Steps	A,I	B	C	D		E	
Forces	D20 D100	D20 D100	D20 D100	D20	D100	D20	D100
N12 (nN)	0	-1.19	-8.96	-1.40E-5	-5.37E-7	0.0016	0.0022
Q13 (nN)	0	4.46	33.46	5.24E-5	2.01E-7	5.72E-5	-0.0004
M12 (fN.m)	0	0	0	0	0	19.2	24.5

Steps	F		G		H	
Forces	D20	D100	D20	D100	D20	D100
N12 (nN)	-1.06	-3.19	2.839	13.08	-1.064	-3.19
Q13 (nN)	3.97	11.93	2.924	7.571	3.97	11.93
M12 (fN.m)	19.2	24.5	42	175	0	0

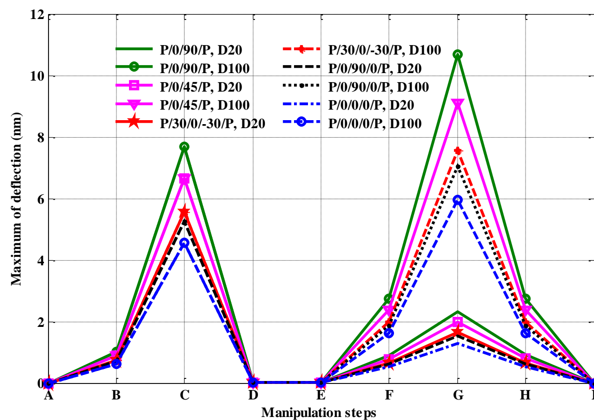

Figure 15. Maximum of MC deflection in various steps of nano-manipulations.

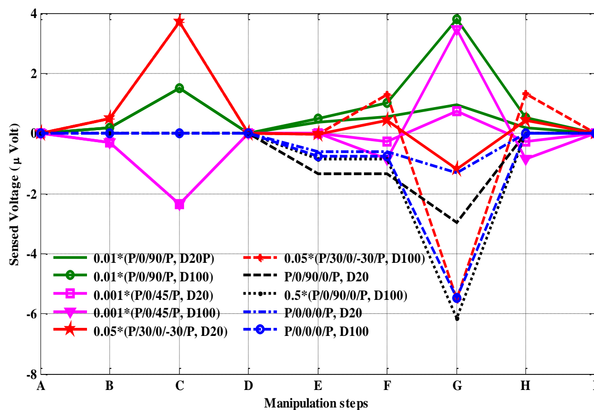

Figure 16. The sensed voltage on the sensor layer of the MC for various lamination.

Figure 16 shows the sensed voltage through the sensor patch on the MC. Consciously, for plotting the diagrams in a specific range, some are multiplied by the coefficients mentioned in the figure legend. The static deflection of regular electromechanical systems has a linear relation with the sensed voltage. Nevertheless, the sensed voltage depends not only on particle size, but also on the structure of the MC. Irregularity can seriously affect the output. The sensed voltage increases with an increase in the particle diameter, but the effects of irregularity cannot be addressed precisely. The egregious discrepancy of the results of P/0/45/P and P/0/90/P from other laminations is illustrated in Figure 16, which demonstrates the effect of irregularity.

5. Conclusions

The precision of nano-imaging and nano-manipulation is an important issue in nano-engineering studies. There are various effective parameters of the quality of images obtained. Parameters of the nano-world are significant but not entirely controllable. However, geometrical and mechanical properties of micro-cantilevers are completely controllable. So, controlling the sensitivity of the resulting image through the lamination design could be a proper approach.

In this paper, semianalytic (GDQ and GDQE methods) static and dynamic solutions of Cartesian laminated beams and plates done to control the results of the nano-metric operations. The semianalytical approach presented is generally based on the FSDT. Comparing the results with the exact and existing numerical approaches revealed its efficiency. After reliable validation, the lamination effects on the static and dynamic manner of micro-cantilevers in nano-metric operations were studied.

Also studied were the nano-imaging effects on the MC shape and the challenges presented by the sensitivity of the resulting image through the lamination. The P/90/0/P lamination resulted in more precision in the ascent, peak and descent of a triangular surface for a substrate. For the square and sinusoidal profiles, image output was completely different. The P/90/0/P lamination led to the worst result. The dependency of the system sensitivity on the profile of a substrate is a highly significant result for imaging especial surfaces. Among all laminations examined, the P/90/0/P and P/0/0/0/P were suggested for triangular and both square and sinusoidal substrates, respectively.

Since piezoelectric shunt damping can be implemented for suppressing vibration in MEMS and NEMS, utilizing the P/30/0/-30/P lamination for scanning simpler substrates, the effects of a proportional damping coefficient on the output were considered. With fewer damping coefficients, even though the triangular and sinusoidal parts were approximately close to the profile of substrate, the ascent and descent parts of square profile were completely different. More damping coefficients led to unwanted delays in the ascents and descents.

Manipulating nanoparticles by using the AFM was studied and by plotting the static deflections and sensed voltage in various steps of manipulation,

it was demonstrated that the bigger the used particle was, the bigger the resulting deflection and voltage were. As the most important result, it was shown that when two mechanical layers were used, the static deflection was greater. The P/0/90/P lamination had the most deflection and the minimum deflection belonged to the P/0/0/0/P lamination. Furthermore, before the step "E" (fifth to nine steps), various laminations led to approximately the same results for various diameters. The sensed voltage depended not only on particle size, but also on the structure of the MC. The sensed voltage increased with an increase in the particle diameter, but the effects of irregularity could not be addressed precisely.

References

[1] Uchino K. Piezoelectric Actuators 2004–Materials, Design, Drive/Control, Modeling and Applications. *Proc 9th Int Conf New Actuators*; 2004.

[2] Lee S, Kim J, Moon W, Choi J, Park I, Bae D. A multibody-based dynamic simulation method for electrostatic actuators. *Nonlinear Dyn* 2008; 54: 53-68.

[3] Lim YH, Varadan VV, Varadan VK. Finite-element modeling of the transient response of MEMS sensors. *Smart Mater Struct* 1997; 6: 53-61.

[4] Beek JV, Puers R. A review of MEMS oscillators for frequency reference and timing applications. *J Micro-mechanics Micro-engineering* 2011; 22: 013001.

[5] Korayem M, Rahneshin V, Sadeghzadeh S. Coarse-grained molecular dynamics simulation of automatic nanomanipulation process: The effect of tip damage on the positioning errors. *Comput Mater Sci* 2012; 60: 201-211.

[6] Korayem M, Rahneshin V, Sadeghzadeh S. Nano cluster manipulation success considering flexibility of system: Coarse grained molecular dynamics simulations. *Scientia Iranica* 2012; 19: 1288-1298.

[7] Darvizeh M, Darvizeh A, Ansari R, Sharma C. Buckling analysis of generally laminated composite plates (generalized differential quadrature rules versus Rayleigh–Ritz method). *Compos Struct* 2004; 63: 69-74.

[8] Hosseini-Hashemi S, Fadaee M, Taher HRD. Exact solutions for free flexural vibration of Lévy-type rectangular thick plates via third-order shear deformation plate theory. *Appl Math Model* 2011; 35: 708-727.

[9] Hashemi SH, Arsanjani M. Exact characteristic equations for some of classical boundary conditions of vibrating moderately thick rectangular plates. *Int J Solids Struct* 2005; 42: 819-853.

[10] Tornabene F. Free vibrations of anisotropic doubly-curved shells and panels of revolution with a free-form meridian resting on Winkler–Pasternak elastic foundations. *Compos Struct* 2011; 94: 186-206.

[11] Balamurugan V, Narayanan S. A piezolaminated composite degenerated shell finite element for active control of structures with distributed piezosensors and actuators. *Smart Mater Struct* 2008; 17: 035031.

[12] Benjeddou A. Advances in piezoelectric finite element modeling of adaptive structural elements: a survey. *Comput Struct* 2000; 76: 347-363.

[13] Tornabene F. 2D GDQ solution for free vibrations of anisotropic doubly-curved shells and panels of revolution. *Compos Struct* 2011; 93: 1854-1876.

[14] Hong C. Computational approach of piezoelectric shells by the GDQ method. *Compos Struct* 2010; 92: 811-816.

[15] Chen C. A differential quadrature element method. *Proc 1st Int Conf Eng Comput Sim*; 1995.

[16] Korayem M, Sadeghzadeh S, Homayooni A. Semi-analytical motion analysis of nano-steering devices, segmented piezotube scanners. *Int J Mech Sci* 2011; 53: 536-548.

[17] Korayem M, Homayooni A, Sadeghzadeh S, Safa M, Rahneshin V. A semi-analytic modeling of nonlinearities for nano-robotic applications, macro and micro sized systems. *2nd Int Conf Control, Instrumentation Automation*; 2011.

[18] Sadeghzadeh S, Korayem MH, Rahneshin V, Homayooni A, Moradi M. **Nanorobotic Applications of Finite Element Method**. Computational Finite Element Methods in Nanotechnology, Editor: Musa S. CRC Press: Taylor and Francis Corporation; 2012.

[19] Sadeghzadeh S, Korayem M, Rahneshin V, Homayooni A. A shape-feedback approach for more precise automatic nano manipulation process. *2nd Int Conf Control, Instrumentation and Automation*; 2011.

[20] Hamed S, Ghader R. Comparison of generalized differential quadrature and Galerkin methods for the analysis of micro-electro-mechanical coupled systems. *Commun Nonlinear Sci Numer Sim* 2009; 14: 2807-2816.

[21] Collinger J, Wickert JA, Corr L. Adaptive piezoelectric vibration control with synchronized switching. *J Dyn Sys Measurement Control* 2009; 131: 041006.